2020 IEEE/ASME International Conference on
Advanced Intelligent Mechatronics (AIM), Boston, USA
(Virtual Conference), July 6-9, 2020

Modelling and Simulation of Pneumatic Sources for Soft Robotic Applications

Matheus S. Xavier, Andrew J. Fleming and Yuen K. Yong[1]

***Abstract*— The mathematical models for two widely used pneumatic systems in the soft robotics community are presented: syringe pumps and compressed air systems. These models enable prediction and optimisation of performance of soft actuators under pressurisation, allowing the user to select pneumatic components for a desired behaviour. Analytical models are confirmed with simulations developed using SimScape Fluids and SimScape Electrical within Simulink/MATLAB. By using a polytropic law, the models show agreement with the simulations with less than 10% discrepancy for the typical pressures used with soft actuators. Syringe pumps are shown to be much slower compared to the compressed air systems. In the latter, the addition of an air receiver allows very short actuation time.**

I. Introduction

The rising interest in soft robots is outlined in recent papers reviewing fabrication procedures [1], biological inspiration [2], actuation methods [3], sensing [4], control [5], stiffening techniques [6] and biomedical applications [7]. The building blocks of soft robots are the soft actuators. One important category of soft actuator is the fluidic elastomer actuator (elastic inflatable actuator), whereby actuation is performed using pneumatics or hydraulics [8]. While these actuators have been extensively used in the literature, the fluid power systems used within the soft robotics community have received less attention. In [9], the authors have compared pneumatic energy sources used in autonomous and wearable soft robots and provided a system-level framework to support the design of untethered pneumatic soft robots, nevertheless the dynamics of actuation is not discussed.

The basic components of a compressed air pneumatic system are the air compressor, the receiver and the valves. Positive displacement compressors are the most widely used and deliver a fixed volume of fluid each cycle, regardless of the pressure at the outlet port [10]. Valves are used to control the direction, flow rate and pressure of the compressed air. The air receiver (storage reservoir or gas tank) is used to store a given volume of compressed air and offers larger system capacity and reduction of pressure changes during short-term demand [11]. The latter is particularly relevant for the intermittent demand commonly experienced in soft robotics. Pressure control in the air receiver is normally achieved using on/off controllers by starting the compressor when the receiver pressure falls below some minimum value and stopping it when pressure rises to a satisfactory level.

The most popular pneumatic control architecture for soft robotics is the fluidic control board [12], an open source hardware platform available from the Soft Robotics Toolkit that was originally employed in the experimental platform of [13], [14]. The board consists mainly of a diaphragm pump and a set of solenoid valves. MOSFETs allow the use of Pulse-Width Modulation (PWM) to control the pressure of fluid passing through the valves. Pressure sensors provide feedback on the behaviour of the system. Basic control options are manually adjusting switches and knobs or automated simple codes running on the included Arduino microcontroller. Advanced control options can be implemented using LabVIEW or Simulink.

Manual pressurisation of syringes, while monitoring the pressure, is the simplest method for evaluation of the behaviour of soft actuators. This method has been employed in characterisation studies to investigate the relation between the geometrical parameters or material characteristics and the bending and extension of soft actuators [15]. Some studies have also used this method to validate FEM results [16]. An automatic alternative is the use of syringe pumps [17]. In order to convert the rotational motion of the motors into linear motion of the syringe plunger, syringe pumps can rely on a rack and pinion [18], [19] or lead screw mechanisms [20]–[22]. In the latter, the motor rotates a threaded rod that drives a nut attached to a 3D printed syringe plunger adapter.

The analytical modelling of syringe pumps has been essentially limited to hydraulic systems. In addition, most models only consider the flow rate being dispensed by the syringe, with no consideration given to pressure dynamics. In [23]–[25], the Poiseuille equation is used to establish the flow rate considering fully developed laminar flow. The flow rate can also be determined by relating the volume of fluid for a single pitch movement and the time required for the rotation [19], [26]. In [27], the authors have used the lumped parameter approach to develop a second-order relation between the output flow rate and velocity of the piston motion for hydraulic fluid (constant bulk modulus).

A. Contributions of this work

In soft robotics, many of the studies using pneumatic control systems are focused in characterisation, in which the speed of actuation is not a concern. However, this is relevant for practical applications of soft robots. While pneumatic energy sources are widely used in soft robotics [9], their modelling has not yet been adequately described. In particular, the modelling of syringe pumps has been limited to the output flow of hydraulic fluids with little attention to pressure dynamics.

Therefore, in this work, the analytical modelling for the two most widely used pneumatic systems in soft robotics are presented: compressed air systems (similar to the fluidic control board) and syringe pumps. The models presented here allow the user to not only predict performance but also to derive component specifications for a given set of soft-robotic performance requirements.

[1]All authors are with the Precision Mechatronics Lab at the School of Electrical Engineering and Computer Science, The University of Newcastle, Callaghan, NSW, Australia {matheus.xavier, andrew.fleming, yuenkuan.yong}@newcastle.edu.au

II. Fundamentals of Pneumatic Systems Modelling

A. Thermodynamic Models for Pneumatic Systems

The following assumptions are considered in this study [28]–[30]: the gas is ideal; pressures and temperature within each control volume are homogeneous; kinetic and potential energy terms are negligible; mass flow rate leakages and viscous work are negligible; and supply and exhaust pressures are constant. As described in [29], the most general thermodynamic model for compressed air systems consists of three equations:

(1) Ideal gas law (equation of state):

$$P = \rho RT \tag{1}$$

where P is the pressure, ρ is the density, R is the ideal gas constant and T is the temperature. For air, $R =$ 287 Nm/(KgK). Further improvement of the pressurisation model can be achieved by considering temperature changes inside the chamber using a polytropic law [30]:

$$T = T_0 \left(\frac{P}{P_0} \right)^{(\gamma-1)/\gamma} \tag{2}$$

(2) Conservation of mass (continuity equation) [31]:

$$\rho_i Q_i - \rho_o Q_o = \frac{d}{dt}(\rho V) \tag{3}$$

where ρ_i and Q_i are the input density and flow rate, ρ_o and Q_o are the output density and flow rate, and ρ and V are the density and volume of the control volume. If a mean density is assumed throughout,

$$Q_i - Q_o = \frac{dV}{dt} + \frac{V}{\rho}\frac{d\rho}{dt} \tag{4}$$

The bulk modulus (β) of a compressible fluid is given by

$$\beta = -V\frac{dP}{dV} = \rho\frac{dP}{d\rho} \Rightarrow \frac{d\rho}{\rho} = \frac{dP}{\beta} \tag{5}$$

Combining the above equations yields

$$Q_i - Q_o = \frac{dV}{dt} + \frac{V}{\beta}\frac{dP}{dt} \tag{6}$$

where $\frac{dV}{dt}$ corresponds to the boundary deformation term and $\frac{V}{\beta}\frac{dP}{dt}$ is the fluid compressibility term. For an isothermal process, $\frac{P}{\rho} = \text{const} \rightarrow \beta = P$. Alternatively, for an isentropic process (adiabatic and reversible), $\frac{P}{\rho^k} = \text{const} \rightarrow \beta = kP$ [32].

(3) Energy equation [29], [33]

$$q_{in} - q_{out} + kC_v(\dot{m}_{in}T_{in} - \dot{m}_{out}T_{out}) - \dot{W} = \dot{U} \tag{7}$$

where q_{in} and q_{out} are the heat transfer terms across the walls, $kC_v(\dot{m}_{in}T_{in} - \dot{m}_{out}T_{out})$ is the net internal energy of the mass flow into the system, $\dot{W} = P\dot{V}$ is the rate of change in the work, and $\dot{U}$ is the change of internal energy. Furthermore, $k = C_p/C_v$ is the specific heat ratio, T_{in} is the temperature of the incoming gas flow, C_p and C_v are the specific heats at constant pressure and volume, respectively.

Assuming the incoming flow has the same temperature as the gas in the chamber ($T_{in} = T$) and adiabatic process ($q_{in} - q_{out} = 0$), the energy equation simplifies to

$$\dot{P} = k\frac{RT}{V}(\dot{m}_{in} - \dot{m}_{out}) - k\frac{P}{V}\dot{V} \tag{8}$$

The general equation for a polytropic process ranging from $\gamma =$ 1 (isothermal process) to $\gamma =$ 1.4 (isentropic process) is given by [29], [30]

$$\dot{P} = \gamma\frac{RT}{V}(\dot{m}_{in} - \dot{m}_{out}) - \gamma\frac{P}{V}\dot{V} \tag{9}$$

For a pneumatic cylinder system, [34] propose that the temperature inside the chamber lays between the theoretical adiabatic curve in the charging process and isothermal curve in the discharging of the chamber. Consequently, a value of $\gamma =$ 1.2 is suggested. According to [9], many soft robots operate below 10 SLM at 100 kPa, hence conditions are polytropic but most likely nearer to isothermal than to adiabatic. Finally, [30] has augmented (9) by considering the heat transfer coefficient between the air inside the control volume and its walls, which only led to a difference of about 10% compared to classical polytropic models.

B. Lumped Parameter Models for Pneumatic Systems

A modelling framework is developed using an energy-based approach to develop lumped parameter models for fluid circuit components [31], [32], [35]. The use of an electrical circuit analogy helps to quickly establish a circuit diagram and is based on the following comparisons: pressure $\leftrightarrow$ voltage and volumetric flow rate $\leftrightarrow$ current. Consequently, fluid capacitance (C), resistance (R) and inertance/inductance (L) are derived as

$$R = \frac{128\mu l}{\pi d_h^4}, \quad C = \frac{V}{\beta}, \quad L = \frac{\rho l}{A} \tag{10}$$

where μ is the dynamic viscosity of the fluid, d_h is the hydraulic diameter, l the length and A the area of the control volume [36]. The hydraulic diameter is simply the diameter for a circular pipe.

III. Air Compressor System

A. Analytical Modelling

In the analytical modelling, five different scenarios with increasing complexity are considered. Firstly, an electrical circuit equivalent is derived for each case. Once a differential equation model is achieved, a pneumatic equivalent description is derived and thermodynamic models are included.

Case 1: Ideal air compressor directly charging actuator.

Here, the air compressor is modelled as a constant volumetric flow rate source with no leakage. The actuator is modelled as a constant volume chamber (V_a). The electrical analog is shown in Fig. 1a. The charging of the capacitor is described by $I = C\frac{dv}{dt}$. For the pneumatic equivalent, $I = Q_c$ (the volumetric flow rate of the air compressor), $C = V_a/(kP_a)$ and $V = P_a$. Therefore,

$$\frac{dP_a}{dt} = \frac{kQ_c}{V_a}P_a \tag{11}$$

Case 2: Real air compressor directly charging actuator.

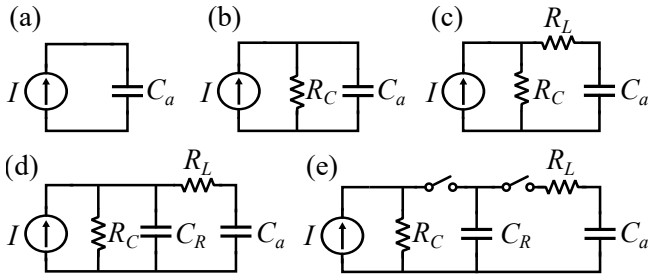

Fig. 1: Electrical analogs of the five cases considered for compressed air systems.

The air compressor is modelled as a constant volumetric flow rate source with leakage (R_C). The electrical analog is shown in Fig. 1b. Using KVL, the charging of the capacitor is described by $I = \frac{v}{R_C} + C\frac{dv}{dt}$. The pneumatic equivalent is

$$Q_c = \frac{P_a}{R_C} + \frac{V_a}{kP_a}\frac{dP_a}{dt} \Rightarrow \frac{dP_a}{dt} = \frac{kQ_C}{V_a}P_a - \frac{k}{V_aR_C}{P_a}^2 \quad (12)$$

Case 3: Real air compressor charging actuator through pipe.

The tube connecting the source and the actuator is modelled as a purely resistive component (R_L). The electrical analog is shown in Fig. 1c. Using KVL, KCL and the component constitutive relations yields the pneumatic equivalent:

$$Q_c = \left(\frac{\frac{R_LV_a}{kP_a} + \frac{R_CV_a}{kP_a}}{R_C}\right)\frac{dP_a}{dt} + \frac{P_a}{R_C} \Rightarrow \frac{dP_a}{dt} = \frac{kQ_C}{\alpha}P_a - \frac{k}{R_C\alpha}{P_a}^2 \quad (13)$$

where $\alpha = \frac{R_LV_a+R_CV_a}{R_C}$.

Case 4: Full system with simultaneous charging of receiver and actuator.

The system is augmented by including an air receiver in the fluid path between the air compressor and actuator. The air receiver is modelled as a constant volume chamber (V_R). The electrical analog is shown in Fig. 1d. Writing the node equations at the receiver and actuator and introducing $C_a = V_a/(kP_a)$, $C_R = V_R/(kP_R)$, $I = Q_c$, $v_R = P_R$ and $v_a = P_a$,

$$\frac{dP_R}{dt} = -\frac{kP_R{}^2}{R_CV_R} - \frac{kP_R{}^2}{R_LV_R} + \frac{kP_RP_a}{R_LV_R} + \frac{kP_RQ_C}{V_R} \quad (14)$$

$$\frac{dP_a}{dt} = \frac{kP_RP_a}{R_LV_a} - \frac{kP_a{}^2}{R_LV_a} \quad (15)$$

Case 5: Full system with pressure control.

Firstly, the air receiver is pressurised by the compressor with no fluid flow allowed between the receiver and actuator. Once the desired pressure is reached, the compressor is turned off and the compressor discharges into the actuator through a valve. The behaviour of the valve and the pressure switch at the receiver are modelled as simple switches in the electrical analog shown in Fig. 1e. In the first scenario, the system has the same configuration as Case 2. In the second scenario, writing the node equations at the receiver and actuator results in the following pneumatic equivalent:

$$\frac{dP_R}{dt} = -\frac{kP_RP_a}{R_LV_R} - \frac{kP_R{}^2}{R_LV_R} \quad (16)$$

$$\frac{dP_a}{dt} = \frac{kP_RP_a}{R_LV_a} - \frac{kP_a{}^2}{R_LV_a} \quad (17)$$

B. Simulation Results

Using the package Simscape Fluids within MATLAB/Simulink, simulations have been developed to analyse the behaviour of the cases previously described. The full system in Case 4 is shown in Fig. 2. In Case 5, the flow rate source and leakage are replaced with an infinite flow resistance and the initial pressure of the receiver is set at its maximum desired pressure, which models the final stage of pressurisation of the receiver. The comparisons between the mathematical and Simulink models are shown in Figs. 3 and 4 with the parameters from Table I.

TABLE I: Parameters for compressed air simulations.

Initial absolute pressure (P_0)	101.325 kPa
Flow rate (Q_C)	6.67e-5 m^3/s (4 LPM)
Diameter of actuator (D_a)	20e-3 m
Length of actuator (L_a)	200e-3 m
Dynamic viscosity of air (μ)	1.849e-5 Pa·s
Length of transmission line (L_l)	0.6 m
Diameter of transmission line (d_l)	5e-3 m
Length of leakage pipe (L_C)	1 m
Diameter of leakage pipe (d_C)	5e-4 m
Volume of air receiver (V_R)	1e-3 m^3 (1 L)
Initial relative pressure of receiver (P_{R0}) in Case 5	300 kPa

The parameters for the transmission line are chosen to match standard 5 mm tubing used with soft actuators. Additionally, the length and diameter of the pipe modelling the leakage of the compressor are selected to obtain a leakage resistance of $\sim 10^{10}\,\mathrm{Nm^{-2}/m^3s^{-1}}$, as suggested in [37].

In Case 1, it is shown that, for a polytropic index of 1.2, the analytical model almost precisely matches the simulations. Throughout Cases 2-5, the actuation process was assumed isothermal. In Cases 2 and 3, a polytropic index of 1.1 has improved the accuracy of the analytical models. Similarly, in Cases 4 and 5, a polytropic index of 1.2 is recommended. Furthermore, in Cases 4 and 5, the transmission line is shown to have great influence in the pressurisation of the actuator and the model does not provide the accurate approximation of the other cases for the 60 cm long pipe. However, reducing the length of the transmission line has improved the accuracy of the model in comparison to the simulations results.

IV. Syringe Pump

A. Analytical Modelling

In the mathematical modelling of the pneumatic syringe pump, the continuity equation is used with $Q_i = 0$, $dV_S/dt = -A_p\dot{x}$, $\beta = kP_S$ and $V_S = V_0 - A_px$, where V_S is the volume of the syringe, P_S is the pressure, A_p is the area of the piston, x is the displacement of the piston and V_0 is the initial volume of the syringe. Hence,

$$A_p\dot{x} - Q_o = \frac{V_0 - A_px}{kP_S}\frac{dP_S}{dt} \quad (18)$$

Using an electrical equivalent and assuming that the transmission line can be modelled as a purely resistive component (R_L), the equation for the output flow is

$$Q_o = \frac{P_S - P_a}{R_L} \quad (19)$$

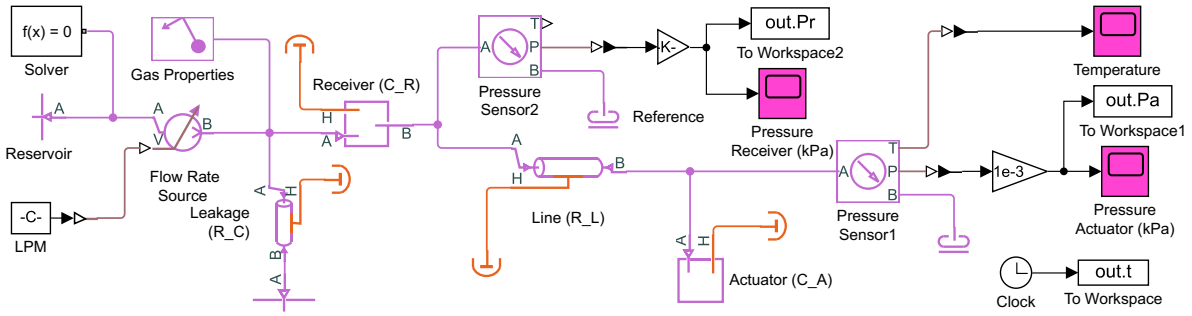

Fig. 2: Modelling of air compressor system in Simulink. The air compressor is modelled as a controlled volumetric flow rate source, the leakage and transmission line are modelled as pipes, and the air receiver and actuator are modelled as constant volume chambers. Pressure sensors are added to the chambers modelling the actuator and receiver.

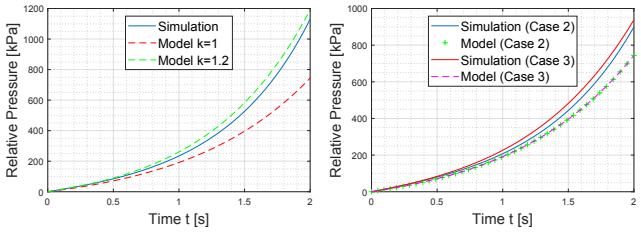

(a) Case 1. (b) Cases 2 and 3.

Fig. 3: Comparison between analytical and Simulink models for Cases 1, 2 and 3.

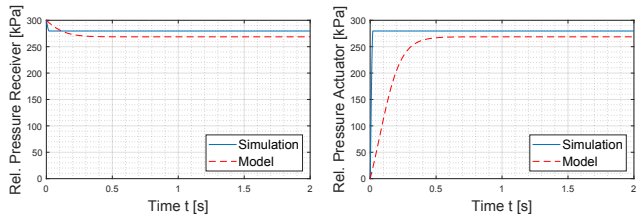

(a) Pressure in the air receiver. (b) Pressure in the actuator.

Fig. 4: Comparison between analytical and Simulink models for Case 5.

where P_a is the pressure of the actuator.

Combining these two equations yields

$$\frac{dP_S}{dt} = \frac{kP_S}{V_0 - A_p x} A_p \dot{x} + \frac{kP_S(P_a - P_S)}{R_L(V_0 - A_p x)} \tag{20}$$

The charging of the actuator from the output flow of the syringe pump is similar to Case 1 and can be written as

$$Q_o = \frac{P_S - P_a}{R_L} = C_a \frac{dP_a}{dt} \Rightarrow \frac{dP_a}{dt} = \frac{kP_a(P_S - P_a)}{R_L V_a} \tag{21}$$

where C_a and V_a are the capacitance and volume of the actuator, respectively.

In addition to the thermodynamic model described above, the modelling of the syringe pump requires an equation of motion for the piston dynamics given by Newton's Law [38]. Neglecting friction,

$$F_m - P_S A_p = m_p \frac{d^2x}{dt^2} \Rightarrow \frac{d^2x}{dt^2} = \frac{F_m}{m_p} - \frac{P_S A_p}{m_p} \tag{22}$$

where F_m is the force provided by the motor and m_p is the mass of the piston. Neglecting losses, energy conservation yields $T_m \omega_m = F_m \dot{x}$, where T_m and ω_m are the torque and angular velocity of the motor, respectively. Equations (20)-(22) can be grouped to form a fourth-order mathematical model of the syringe pump.

Considering a syringe pump with lead screw mechanism, the linear velocity of the plunger is related to the angular velocity of the motor by

$$\dot{x} = \frac{p}{2\pi} \omega_m \tag{23}$$

where p is the pitch of the screw [39]. The majority of syringe pump designs employ a stepper motor. In this case, the angular velocity of the motor is controlled by the stepping rate (f), which corresponds to the number of steps per second [40], as given by

$$\omega_m = \frac{2\pi f}{N_{rev}} \tag{24}$$

where N_{rev} is the number of steps per revolution.

A simplified model can be achieved by considering the stepper motor as constant source of angular velocity ("slewing" operation). From equations (23) and (24), $\dot{x} = \frac{pf}{N_{rev}}$, resulting in the following third-order model:

$$\dot{P}_S = \frac{kA_p pf}{N_{rev}(V_0 - A_p x)} P_S + \frac{kP_S(P_a - P_S)}{R_L(V_0 - A_p x)} \tag{25}$$

$$\dot{P}_a = \frac{kP_a(P_S - P_a)}{R_L V_a} \tag{26}$$

$$\dot{x} = \frac{p}{2\pi} \omega_m \tag{27}$$

B. Simulation Results

Using the packages Simscape Fluids and Simscape Electrical, simulations have been developed to analyse the behaviour of the syringe pump and for comparison to the simplified mathematical model in (25)-(27). The full model is shown in Fig. 5. The comparison between the mathematical and Simulink models is shown in Fig. 6a. The parameters for the actuator and line are kept as before, while the additional parameters are listed in Table II.

V. Pneumatic Sizing

In this section, a method to determine the sizing of pneumatic components for a required application is developed.

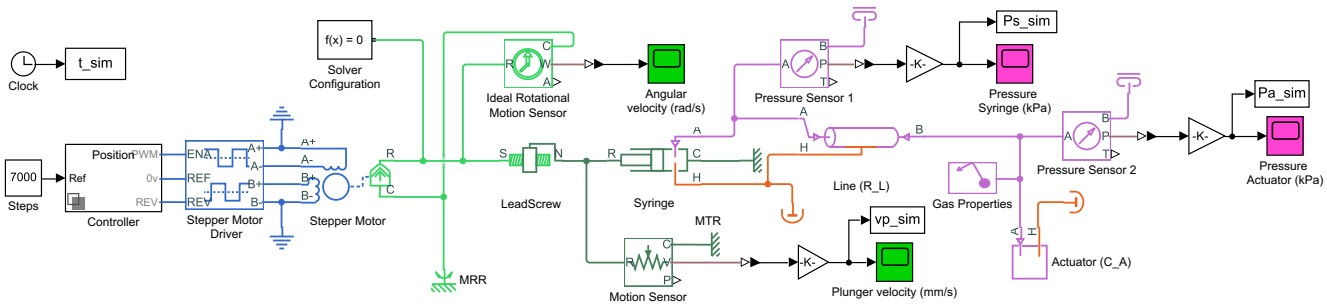

Fig. 5: Modelling of pneumatic syringe pump in Simulink. The motor driver takes the stepping rate and number of steps as inputs to drive the stepper motor. Rotational motion of the motors is converted into linear motion of the syringe plunger via a lead screw mechanism. The syringe pump is modelled as a translational mechanical converter, the transmission line as a pipe and the actuator as a constant volume chamber.

TABLE II: Parameters for syringe pump simulations.

Initial volume of syringe (V_0)	6e-5 m^3 (60 mL)
Diameter of piston (D_p)	29e-3 m
Length of syringe (L_s)	90e-3 m
Stepping rate (f)	700 steps/s
Number of steps/rev (N_{rev})	200
Pitch of screw (p)	1.25e-3 m
Polytropic index (γ)	1.2

Firstly, a method to determine the required stepping rate for a desired pressure and actuation time is shown in Fig. 6a. A 60 mL syringe with the same parameters as in the previous section is used and the stepping rate is varied from 300 to 900 steps/s. The dynamics of a syringe pump actuated by a stepper motor is strongly dependent on the velocity of the piston, which is controlled by the stepping rate. The actuation speed can be increased by using higher values of the stepping rate. The maximum stepping rate of the motor can be calculated using the maximum flux linkage in each winding [40]. For the standard stepper motor in Simulink, the maximum rate is approximately 780 steps/s.

Here, Case 3 is considered to evaluate the charging of an actuator. The user-defined parameters are the volume of the actuator and the line and leakage parameters. In Fig. 6b, the pressurisation of a cylindrical actuator with 20 mm diameter and 200 mm height is shown for a range of input flow rates. Using Fig. 6b, the required air compressor can be determined for the desired pressure and actuation time. Note that the length of the transmission line has great influence in the delay between actuation and pressurisation, with longer pipes resulting in increased actuation time.

On the other hand, with the inclusion of air receiver, the user-defined parameters become the air receiver size and initial pressure, besides the volume of the actuator and line parameters. In this situation, Case 5 is used to simulate the post-pressurisation stage of the receiver. In Fig. 6c, a receiver of 1 L is used and the initial relative pressure is varied from 50 kPa to 300 kPa. It is clear that the addition of a receiver leads to very short actuation time. Alternatively, a sweep on the receiver volume at a fixed initial pressure reveals that higher volumes result in smaller pressure variations in the receiver. Using the modelling for Case 5, the receiver discharges until its pressure equals the actuator pressure. However, in a practical system, the valves would close once the desired pressure of the actuator is reached and no further discharging would be allowed. Hence, Fig. 6c serves as a reference to how fast the desired pressure can be reached.

VI. Conclusions and Future Work

In this work, two widely used pneumatic systems within the soft robotics community are analysed. By using a polytropic law, the analytical models show agreement with the simulations within a 10% error for the typical pressures used with soft actuators, i.e. below 500 kPa. The results also show that syringe pumps are much slower solutions in comparison to compressed air systems, which is a potential limitation for practical implementation of soft robots. In the latter, the addition of an air receiver allows very fast pressurisation of the soft actuators.

The mathematical models developed here allow the user to not only predict the pressurisation behaviour but also to decide on which pneumatic components are required for desired performance. In particular, the user is able to select air compressors and air receivers (for the compressed air system) or stepping rates (for the syringe pumps) satisfying the rise of actuator's pressure within a desired timeframe. The pneumatic models can be easily modified to accomodate hydraulic fluids by simply assuming constant bulk modulus. Future work includes the experimental validation of the analytical models and simulations.

Acknowledgment

The authors would like to thank Annabelle Farnworth for the useful discussions regarding the compressed air system.

References

[1] F. Schmitt, O. Piccin, L. Barbé, and B. Bayle, "Soft robots manufacturing: a review," *Frontiers in Robotics and AI*, vol. 5, p. 84, 2018.
[2] S. Kim, C. Laschi, and B. Trimmer, "Soft robotics: A bioinspired evolution in robotics," *Trends in Biotechnology*, vol. 31, no. 5, pp. 287–294, 2013.
[3] P. Boyraz, G. Runge, and A. Raatz, "An overview of novel actuators for soft robotics," vol. 7, no. 3, p. 48, 2018.
[4] H. Wang, M. Totaro, and L. Beccai, "Toward perceptive soft robots: Progress and challenges," *Advanced Science*, vol. 5, no. 9, p. 1800541, 2018.
[5] D. Rus and M. Tolley, "Design, fabrication and control of soft robots," *Nature*, vol. 521, no. 7553, pp. 467–475, 2015.
[6] M. Manti, V. Cacucciolo, and M. Cianchetti, "Stiffening in soft robotics: A review of the state of the art," *IEEE Robotics & Automation Magazine*, vol. 23, no. 3, pp. 93–106, 2016.

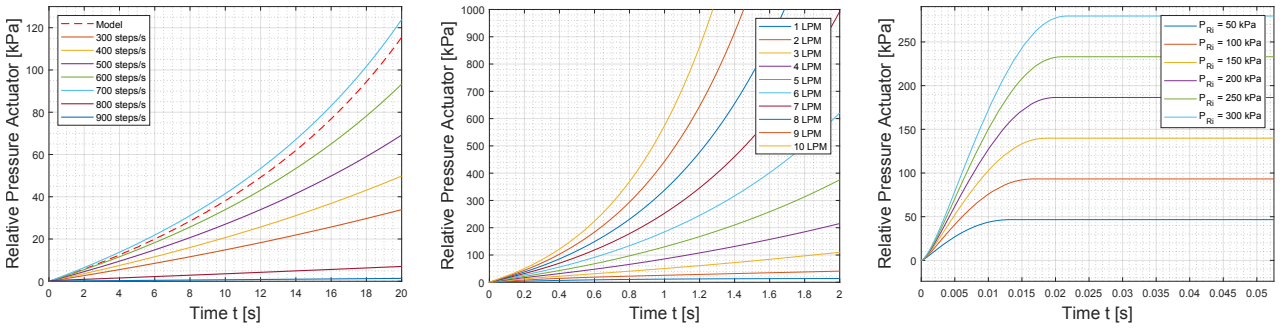

(a) Syringe pump. (b) Compressed air system (Case 3). (c) Compressed air system (Case 5).

Fig. 6: Comparison of performance of syringe pump and compressed air system in the pressurisation of a cylindrical actuator. In (a), the the analytical model for 700 steps/s and Simulink model for a range of stepping rates from 300 steps/s to 900 steps/s are shown. In (b), the pressurisation with the compressed air system for input flow rates from 1 LPM to 10 LPM is shown. In (c), the pressurisation using a 1 L air receiver with initial pressures varying from 50 kPa to 300 kPa is plotted.

[7] M. Cianchetti, C. Laschi, A. Menciassi, and P. Dario, "Biomedical applications of soft robotics," *Nature Reviews Materials*, vol. 3, no. 6, pp. 143–153, 2018.

[8] B. Gorissen, D. Reynaerts, S. Konishi, K. Yoshida, J.-W. Kim, and M. De Volder, "Elastic inflatable actuators for soft robotic applications," *Advanced Materials*, vol. 29, no. 43, 2017.

[9] M. Wehner, M. T. Tolley, Y. Mengüç, Y.-L. Park, A. Mozeika, Y. Ding, C. Onal, R. F. Shepherd, G. M. Whitesides, and R. J. Wood, "Pneumatic energy sources for autonomous and wearable soft robotics," *Soft robotics*, vol. 1, no. 4, pp. 263–274, 2014.

[10] A. Parr, *Hydraulics and pneumatics: a technician's and engineer's guide*. Elsevier, 2011.

[11] J. T, *Pneumatics: Concepts, Design and Applications*. Universities Press, 2015.

[12] "Soft robotics toolkit," 2019, retrieved on 27/03/2019. [Online]. Available: https://softroboticstoolkit.com/components

[13] P. Polygerinos, S. Lyne, Z. Wang, L. Nicolini, B. Mosadegh, G. Whitesides, and C. Walsh, "Towards a soft pneumatic glove for hand rehabilitation," in *Proceedings - IEEE International Conference on Intelligent Robots and Systems*, 2013, pp. 1512–1517.

[14] K. Galloway, P. Polygerinos, C. Walsh, and R. Wood, "Mechanically programmable bend radius for fiber-reinforced soft actuators," in *Proceedings - International Conference on Advanced Robotics*, 2013.

[15] M. S. Xavier, A. J. Fleming, and Y. K. Yong, "Experimental characterisation of hydraulic fiber-reinforced soft actuators for worm-like robots," in *Proceedings - International Conference on Control, Mechatronics and Automation (ICCMA)*. IEEE, 2019, pp. 204–209.

[16] G. Decroly, B. Mertens, P. Lambert, and A. Delchambre, "Design, characterization and optimization of a soft fluidic actuator for minimally invasive surgery," *International journal of computer assisted radiology and surgery*, pp. 1–8, 2019.

[17] B. Wijnen, E. Hunt, G. Anzalone, and J. Pearce, "Open-source syringe pump library," *PLoS ONE*, vol. 9, no. 9, 2014.

[18] K. Ikuta, Y. Matsuda, D. Yajima, and Y. Ota, "Pressure pulse drive: A control method for the precise bending of hydraulic active catheters," *IEEE/ASME Transactions on Mechatronics*, vol. 17, no. 5, pp. 876–883, 2012.

[19] K. Akash, S. Sangavi, and M. Venkatesan, "Double acting syringe pump using a rack and pinion mechanism—simulink model," in *2016 IEEE International Conference on Computational Intelligence and Computing Research (ICCIC)*. IEEE, 2016, pp. 1–4.

[20] T. Kalisky, Y. Wang, B. Shih, D. Drotman, S. Jadhav, E. Aronoff-Spencer, and M. Tolley, "Differential pressure control of 3d printed soft fluidic actuators," in *Proceedings - IEEE International Conference on Intelligent Robots and Systems*, 2017, pp. 6207–6213.

[21] J. Lake, K. Heyde, and W. Ruder, "Low-cost feedback-controlled syringe pressure pumps for microfluidics applications," *PLoS ONE*, vol. 12, no. 4, 2017.

[22] M. S. Xavier, A. J. Fleming, and Y. K. Yong, "Image-guided locomotion of a pneumatic-driven peristaltic soft robot," in *Proceedings - IEEE International Conference on Robotics and Biomimetics (ROBIO)*. IEEE, 2019, pp. 2269–2274.

[23] I. Saidi, L. A. Ouni, and M. Benrejeb, "Design of an electrical syringe pump using a linear tubular step actuator," *International Journal of Sciences and Techniques of Automatic Control & Corn puler Engineering*, pp. 1388–1401, 2010.

[24] W. Zeng, I. Jacobi, D. J. Beck, S. Li, and H. A. Stone, "Characterization of syringe-pump-driven induced pressure fluctuations in elastic microchannels," *Lab on a Chip*, vol. 15, no. 4, pp. 1110–1115, 2015.

[25] P. Karimaghaee, A. Hosseinzadeh, A. Amidi, and E. Roshandel, "Adaptive control application on syringe pump pressure control systems in oil and gas industries," in *2017 5th International Conference on Control, Instrumentation, and Automation (ICCIA)*. IEEE, 2017, pp. 259–264.

[26] M. Appaji, G. S. Reddy, S. Arunkumar, and M. Venkatesan, "An 8051 microcontroller based syringe pump control system for surface micromachining," *Procedia Materials Science*, vol. 5, pp. 1791–1800, 2014.

[27] X. Chen and J. Kai, "Modeling of positive-displacement fluid dispensing processes," *IEEE transactions on electronics packaging manufacturing*, vol. 27, no. 3, pp. 157–163, 2004.

[28] T. Sénac, A. Lelevé, R. Moreau, C. Novales, L. Nouaille, M. T. Pham, and P. Vieyres, "A review of pneumatic actuators used for the design of medical simulators and medical tools," *Multimodal Technologies and Interaction*, vol. 3, no. 3, p. 47, 2019.

[29] E. Richer and Y. Hurmuzlu, "A high performance pneumatic force actuator system: Part i—nonlinear mathematical model," *Journal of Dynamic Systems, Measurement, and Control*, vol. 122, no. 3, pp. 416–425, 2000.

[30] J. F. Carneiro and F. G. de Almeida, "Reduced-order thermodynamic models for servo-pneumatic actuator chambers," *Proceedings of the Institution of Mechanical Engineers, Part I: Journal of Systems and Control Engineering*, vol. 220, no. 4, pp. 301–314, 2006.

[31] J. Watton, *Fluid power systems: modeling, simulation, analog and microcomputer control*. Prentice-Hall, Inc., 1989.

[32] C. W. De Silva, *Mechatronics: an integrated approach*. CRC press, 2004.

[33] S. Liu and J. E. Bobrow, "An Analysis of a Pneumatic Servo System and Its Application to a Computer-Controlled Robot," *Journal of Dynamic Systems, Measurement, and Control*, vol. 110, no. 3, pp. 228–235, 1988.

[34] A. M. Al-Ibrahim, *Transient air temperature and pressure measurements during the charging and discharging processes of an actuating pneumatic cylinder*. University of Wisconsin–Madison, 1991.

[35] D. C. Karnopp, D. L. Margolis, and R. C. Rosenberg, *System dynamics: modeling, simulation, and control of mechatronic systems*. John Wiley & Sons, 2012.

[36] D. Hullender and R. Woods, "Modeling of fluid control components," in *Integral methods in science and engineering*. Springer-Verlag, 1986, pp. 608–619.

[37] J. Watton, *Modelling, monitoring and diagnostic techniques for fluid power systems*. Springer Science & Business Media, 2007.

[38] J. Wang, J. Pu, and P. Moore, "A practical control strategy for servo-pneumatic actuator systems," *Control Engineering Practice*, vol. 7, no. 12, pp. 1483–1488, 1999.

[39] R. Eggert, "Power screws," *Standard handbook of machine design*, 1996.

[40] P. P. Acarnley, *Stepping motors: a guide to theory and practice*. Iet, 2002, no. 63.